Garnet-Type Lithium Metal Fluorides: A Potential Solid Electrolyte for Solid-State Batteries

Ediga Umeshbabu,* Satyanarayana Maddukuri, Doron Aurbach, Maximilian Fichtner,* and Anji Reddy Munnangi*

ABSTRACT: In this work, we introduced a garnet-type lithium metal fluoride, $Li_3Na_3M_2F_{12}$ (M = Al, Sc, In), as solid-state lithium-ion conductors for the first t ime. T he m echanically milled $Li_3Na_3M_2F_{12}$ compounds crystallized in a cubic garnet-like structure ($Ia\bar{3}d$, No. 230). The ionic conductivities of $Li_3Na_3Al_2F_{12}$, $Li_3Na_3Sc_2F_{12}$, and $Li_3Na_3In_2F_{12}$ are 1.7×10^{-6}, 8.2×10^{-6}, and 2.4×10^{-6} S/cm at 300 °C and 1.2×10^{-10}, 2.6×10^{-9}, and 1.8×10^{-10} S/cm at 100 °C, respectively. Even though these fluoride g arnets' c onductivity i s l ess, i t i s s till b etter than those of the oxide analogues $Li_3Ln_3Te_2O_{12}$ (Ln = Er, Gd, Tb, Nd). Moreover, we explored why garnet-type $Li_3Na_3M_2F_{12}$ has low ionic conductivity and presented strategies for further improving conductivities.

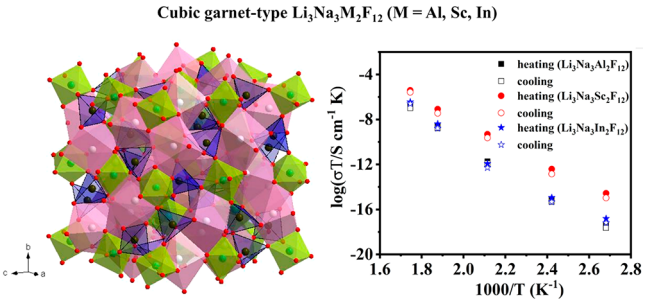

KEYWORDS: *Garnet-type lithium metal f luorides, Solid electrolytes, XRD, Rietveld ref inement, Ionic conductivity, Solid-state lithium batteries*

Solid-state batteries (SSBs) promise high specific and volumetric energy densities, and greater safety.[1] Nevertheless, SSBs face several inherent issues hindering their development. SSBs use solid-state electrolytes (SEs) to shuttle ions between positive and negative electrodes.[2] These SEs can be broadly categorized into ceramic SEs based on oxide and phosphate materials and glass-type SEs (sulfide-based materials).[2−4] These SEs have distinct advantages over the flammable organic liquid electrolyte, such as higher safety and enhanced thermal stability. Furthermore, these SEs have a higher Li^+ transference number ($t_{Li^+} \approx 1$) than aprotic electrolytes ($t_{Li^+} \approx 0.2-0.5$), which significantly improves electrode concentration polarization.[2,3] Ceramic SEs exhibit high bulk conductivity and provide high chemical and electrochemical stability. However, due to their high mechanical rigidity, ceramic SEs are challenging to integrate into SSBs.[3] Sulfide-based SEs are easily incorporated into SSBs due to their mechanical properties and their high ionic conductivity ($10^{-2}-10^{-3}$ S/cm).[3,5] However, sulfide-based SEs suffer from low chemical and electrochemical stability. Both ceramic and glassy-type SEs exhibit interfacial issues with both anodes and cathodes.[4,5] Electronic conductivity can be induced in both SEs upon further inserting or reacting with a lithium metal anode.

We recently discovered that fluoride-based SEs are essentially part of the halide family and can be classified as third-type ionic conducting SEs and offer distinct advantages over ceramic and glassy SEs.[6] Using β-Li_3AlF_6, we have highlighted the benefits of fluoride-based SEs. Several other fluoride-based SEs, such as Li_3MF_6 (Ga, In, Sc), Li_2ZrF_6, $LiScF_4$, $LiYF_4$, and $LiAlF_4$, have been reported.[7−9] The fluoride-based SEs substantiate high electro(chemical) stability against Li metal anode and excellent mechanical properties. Another unique advantage of fluoride-based SEs is that all metal fluorides are intrinsic insulators. Even in the event of Li insertion or reaction, fluoride-based SEs remain electrical insulators. While there are these several advantages to fluoride-based SEs, the ionic conductivity of fluoride-based SEs is generally low and needs improvement for the intended applications in SSBs. Recently, chloride- and bromide-based SEs have been reported in this line.[10] Even though these SEs show higher ionic conductivity than fluoride SEs, the chemical and electrochemical stabilities are a great concern. In continuing to develop fluoride-based SEs for SSBs, herein we explore a new class of garnet-type lithium metal fluorides for the first time, $Li_3Na_3M_2F_{12}$ (M = Al, Sc, In), as a potential SEs for solid-state lithium batteries.

Garnet-type compounds with the general formula $X_3Y_2(SiO_4)_3$ are well-known, and the garnet structure is versatile.[11] The X and Y sites are usually occupied by divalent

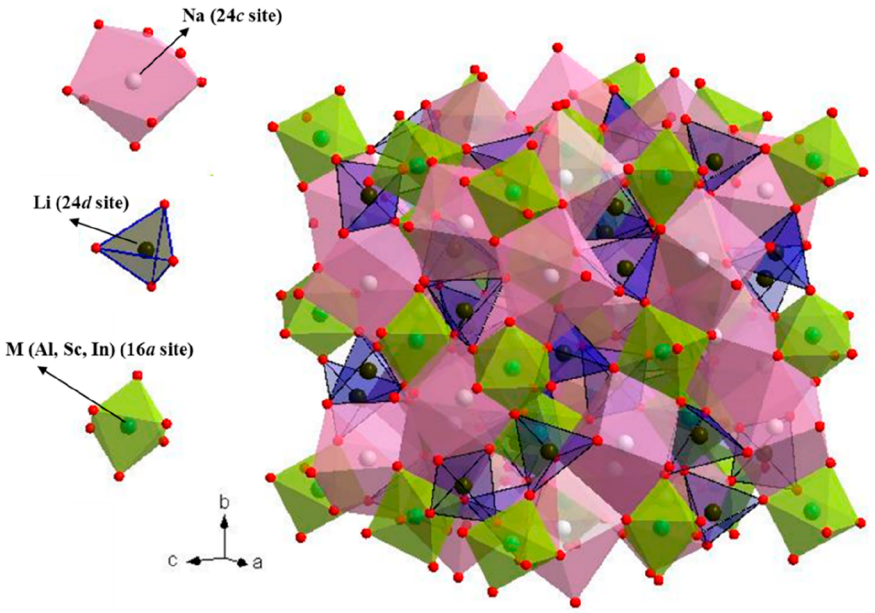

Figure 1. Crystal structural of cubic garnet-type $Li_3Na_3M_2F_{12}$ (M = Al, Sc, In) and the local coordination environment of M^{3+}, Li^+, and Na^+ ions.

(Ca, Mg, or Fe)$^{2+}$ and trivalent (Al, Fe, or Cr)$^{3+}$ cations. Lithium-containing garnet-type compounds are well-known and have been explored extensively for their ionic conductivity.[12−14] These compounds exhibit a three-dimensional network of Li ions and have low activation barriers for Li^+ jumps, an ideal precondition for SE applications. The ionic conductivity of Li-containing oxide garnets varies significantly with Li content and doping (X and Y sites).[15,16] These interesting properties found in Li garnets led us to search for fluoride-equivalent garnets. Indeed, lithium-containing fluoride garnets are known for their luminescent properties.[17] Herein, we investigate the Li ionic conducting properties of three distinct metal-based garnet-structured fluorides, namely, $Li_3Na_3Al_2F_{12}$, $Li_3Na_3Sc_2F_{12}$, and $Li_3Na_3In_2F_{12}$.

The mechanical ball-milling process has been used to synthesize $Li_3Na_3M_2F_{12}$ (M = Al, Sc, In) garnet, and the detailed synthesis procedure is given in the Experimental Section in the Supporting Information. Among these, $Li_3Na_3Al_2F_{12}$ and $Li_3Na_3In_2F_{12}$ are known.[17,18] $Li_3Na_3Sc_2F_{12}$ is a new compound. All three compounds have a cubic garnet-type structure with space group $Ia\bar{3}d$ (No. 230). The ideal garnet crystal structure of $Li_3Na_3M_2F_{12}$ is shown in Figure 1. Here, M^{3+} ions occupy octahedral 16*a* sites; in contrast, the Na^+ ions occupy the dodecahedral 24*c* sites and Li^+ ions exactly fill the tetrahedrally coordinated sites (24*d*), leaving the octahedrally coordinated site vacant. The fluoride ions (red dots) at the corners of the MF_6 octahedra (green color shaded) are shared with the LiF_4 tetrahedra (blue color shaded) and vice versa. The monovalent Na^+ ions (pink color shaded) occupy three-dimensionally distribution in dodecahedral sites.

To confirm phase purity, the as-prepared samples' XRD data were initially verified with the standard ICSD XRD patterns. Supporting Information Figure S1 compares powder XRD patterns with standard ICSD patterns of $Li_3Na_3Al_2F_{12}$, $Li_3Na_3Sc_2F_{12}$, and $Li_3Na_3In_2F_{12}$. All three compounds possess well-defined diffraction peaks that could be indexed to cubic structure with space group $Ia\bar{3}d$ (230). For the $Li_3Na_3In_2F_{12}$ sample, peaks of minor unknown impurities are observed. To further identify the crystal structure, we have applied the structural analysis method using GSAS Rietveld refinement for $Li_3Na_3M_2F_{12}$ (M = Al, Sc, In) compounds and studied crystal lattice and cell parameters. An exemplary refinement (with tabulated data) for all three compounds is shown in Figure 2. The refined lattice constants typically range from 12.14 to 12.81 Å. In addition, smaller χ^2 and *R*-factors are achieved in all three compound refinements, suggesting Rietveld refinement delivers a good fit to the experimental data. From powder XRD data, theoretical densities (ρ_{theo}) for $Li_3Na_3Al_2F_{12}$, $Li_3Na_3Sc_2F_{12}$, and $Li_3Na_3In_2F_{12}$ are calculated to be 2.75, 3.53, and 2.66 g/cm^3, respectively. The relative densities for corresponding samples are in the range of 87−91%.

Figure S3 shows SEM images of the as-prepared fluoride garnets and their corresponding elemental mapping. As seen from the pictures, all three compounds exhibit irregular surface morphology and particles are agglomerated largely owing to expeditious ball-milling for an extended period. The elemental mapping results by EDS (Figure S3) confirm the uniform distributions of Na, F, and Al/Sc/In elements in the ball-milled products. The particle size distributions of all three compounds were estimated using a laser particle analyzer (details are provided in the Experimental Section), and corresponding results are shown in Figure S4 and Table S1. The results show that all three samples have trimodel particle size distribution, with mean particle size distributions (D_{50}) of 12.80, 4.24, and 5.40 m for $Li_3Na_3Al_2F_{12}$, $Li_3Na_3Sc_2F_{12}$, and $Li_3Na_3In_2F_{12}$, respectively. During high-energy ball-milling, particle agglomeration occurred in all three samples, which led to the large particle sizes observed. These findings are in good agreement with those of the SEM results. We examined the structural stability of as-prepared compounds by soaking powder samples in water. The results (Figure S5) indicate that all three fluoride garnets did not change their structure.

Thermogravimetric analysis (TGA) was performed to evaluate the thermal characteristics of ball-milled products, and the corresponding profiles are presented in Figure 3. It can

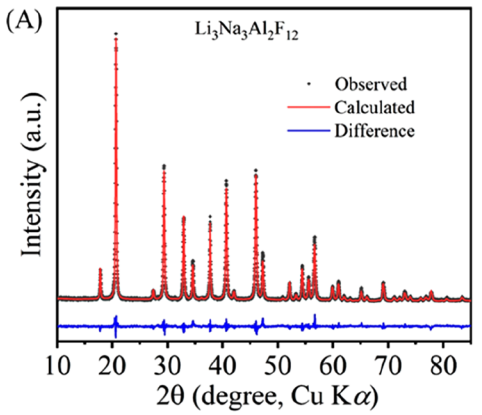

Refined structural parameters for $Li_3Na_3Al_2F_{12}$ (Cubic, SG: *Ia-3d (230)*)

Atom	Wyck. position	*x*	*y*	*z*	U_{iso} (Å²)
Na	*24c*	1/8	0	1/4	0.0290(3)
Li	*24d*	3/8	0	1/4	0.0290(3)
Al	*16a*	0	0	0	0.0290(3)
F	*96h*	0.029174	0.043301	0.639732	0.0290(3)

Refinement lattice parameters: $a = b = c = 12.1489(1)$, and $V = 1793.15(4)$ Å³

Refined factors: $\chi^2 = 1.19$, $R_{wp} = 0.11$ and $R_p = 0.08$

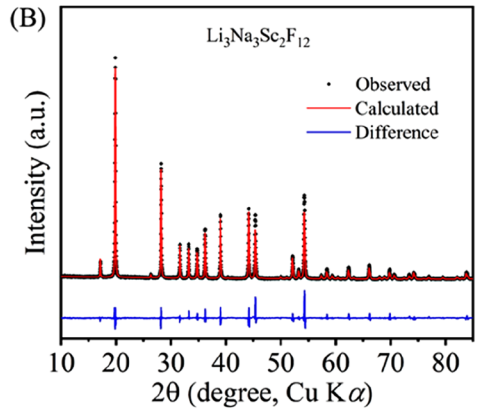

Refined structural parameters for $Li_3Na_3Sc_2F_{12}$ (Cubic, SG: *Ia-3d (230)*)

Atom	Wyck. position	*x*	*y*	*z*	U_{iso} (Å²)
Na	*24c*	1/8	0	1/4	0.0279(5)
Li	*24d*	3/8	0	1/4	0.0279(5)
Sc	*16a*	0	0	0	0.0279(5)
F	*96h*	0.029793	0.048191	0.648755	0.0279(5)

Refinement lattice parameters: $a = b = c = 12.6398(1)$, and $V = 2019.39$ (4) Å³

Refined factors: $\chi^2 = 2.3$, $R_{wp} = 0.14$ and $R_p = 0.11$

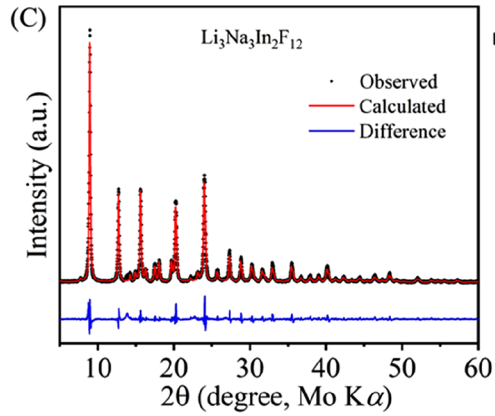

Refined structural parameters for $Li_3Na_3In_2F_{12}$ (Cubic, SG: *Ia-3d (230)*)

Atom	Wyck. position	*x*	*y*	*z*	U_{iso} (Å²)
Na	*24c*	1/8	0	1/4	0.0109(2)
Li	*24d*	3/8	0	1/4	0.0109(2)
In	*16a*	0	0	0	0.0109(2)
F	*96h*	0.029679	0.050546	0.652551	0.0109(2)

Refinement lattice parameters: $a = b = c = 12.7189(2)$, and $V = 2057.52$ (11) Å³

Refined factors: $\chi^2 = 2.65$, $R_{wp} = 0.118$ and $R_p = 0.091$

Figure 2. X-ray Rietveld refinement results and refined structural parameters for (A) $Li_3Na_3Al_2F_{12}$, (B) $Li_3Na_3Sc_2F_{12}$, and (C) $Li_3Na_3In_2F_{12}$.

be seen from the TGA curves that all three fluoride garnets were stable up to 650 °C. The significant weight loss occurs beyond 650 °C, corresponding to the cubic garnet phase decomposition. In contrast to Al- and In-based garnets, the Sc-based garnet shows an additional weight loss below 200 °C, ascribed to the decomposition of unknown impurities. However, it is worth noting that fluoride garnets show lower thermal stability compared to oxide-based garnet structures. This could be because of the difference in bond strengths and resilience of M−F, Li−F, and Na−F bonds compared to those of M−O−M and Li−O bonds in oxide garnets.[19]

AC impedance spectroscopy was performed to investigate the lithium ionic conductivity of fluoride garnets $Li_3Na_3M_2F_{12}$ (M = Al, Sc, In) over a wide frequency and temperature range. Figure 4A shows Nyquist plots of $Li_3Na_3Al_2F_{12}$, $Li_3Na_3Sc_2F_{12}$, and $Li_3Na_3In_2F_{12}$ recorded at 300 °C. The experimental impedance data of samples fitted to an equivalent circuit are illustrated in the inset of Figure 4A. The semicircles are modeled by a resistor and capacitor in parallel and a spike as a capacitor. All three compounds showed different behavior in their profiles depending on material properties.[20] For instance, $Li_3Na_3Al_2F_{12}$ and $Li_3Na_3Sc_2F_{12}$ exhibit two semicircles in the high- to medium-frequency ranges, while $Li_3Na_3In_2F_{12}$ showed only one semicircle. The high-frequency semicircle(s) correspond to bulk and grain boundary contributions. At the same time, a spike in the low-frequency region is attributed to Li^+-ion blocking behavior at the electrode/SEs interfaces.[21−23] Figures 4A and S6 compare the Nyquist plots collected at various temperatures. At 100 °C, the spectra of all three compounds consist of a single semicircle, and a low-frequency spike appears as the temperature increases. Since the contact between the Au-blocking electrode and solid electrolyte (such as fluoride garnets) gets better with temperature, therefore, a low-frequency tail (typical of ionic conduction using blocking electrodes) is expected to form as the temperature rises. Similar characteristic behavior is observed in the literature.[21,24]

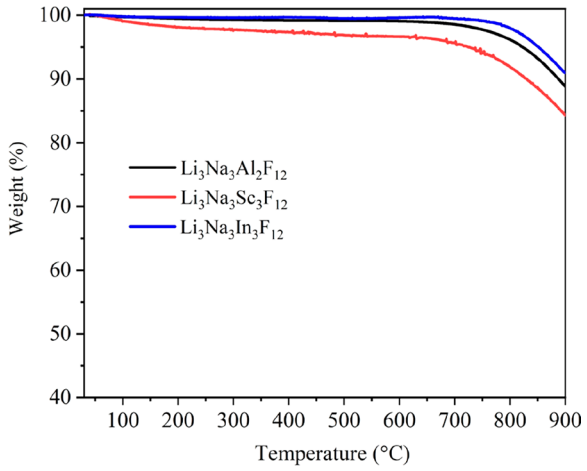

Figure 3. TGA curves of the ball-milled products of $Li_3Na_3Al_2F_{12}$, $Li_3Na_3Sc_2F_{12}$, and $Li_3Na_3In_2F_{12}$.

Sc- and Al-based compounds, on the other hand, showed additional semicircles when the temperature of the cell increased above 260 °C. It is noticed that a decrease in total resistance was observed with an increase in temperature in all three compounds owing to an increase in Li-ion mobility.[25]

The calculated Li^+ ionic conductivities for three different fluoride garnets measured at diverse temperatures are shown in Table 1. At 300 °C, $Li_3Na_3Al_2F_{12}$, $Li_3Na_3Sc_2F_{12}$, and $Li_3Na_3In_2F_{12}$ compounds show maximum conductivity of 1.7×10^{-6}, 8.2×10^{-6}, and 2.4×10^{-6} S/cm, respectively. These values decrease as temperature decreases. When the temperature is reduced to 100 °C, the retained conductivity for $Li_3Na_3Al_2F_{12}$ and $Li_3Na_3In_2F_{12}$ is around 10^{-10} S/cm, and it is 10^{-9} S/cm for $Li_3Na_3Sc_2F_{12}$. All three compounds have no measurable lithium ionic conductivity at room temperature (RT). In the conventional lithium garnet frameworks, $Li_3Ln_3Te_2O_{12}$ (Ln = Y, Pr, Nd, Sm–Lu), all lithium ions occupy the tetrahedrally coordinated site (24d), leaving the octahedrally coordinated site vacant.[12] As a result, there is no room for the mobility of Li ions between $Li_3Na_3M_2F_{12}$ slabs. Therefore, the ionic conductivity at RT for the Li_3-based garnet compositions was immeasurably small. A similar behavior, i.e., lack of RT ionic conductivity was reported in Ruddlesden–Popper oxides.[25] The Li^+ conductivity improved with the increase in cell temperature. At 100 °C, it reached 10^{-10} S/cm for $Li_3Na_3Al_2F_{12}$ and $Li_3Na_3In_2F_{12}$ and 10^{-9} S/cm for $Li_3Na_3Sc_2F_{12}$ and eventually crossed the ionic conductivity of 10^{-6} S/cm at 300 °C because of the increased mobility of lithium ions at elevated temperatures.[21,22] The ionic conductivities of our fluoride garnet compounds are higher than the reported oxide garnets, and Ruddlesden–Popper-type oxides, as listed in Table S2. The calculated electrical conductivities for $Li_3Na_3Al_2F_{12}$, $Li_3Na_3Sc_2F_{12}$, and $Li_3Na_3In_2F_{12}$ using DC polarization are 2.1×10^{-8}, 7.6×10^{-8}, and 6.9×10^{-8} S/cm, respectively, at 300 °C (Figure S7).

Arrhenius plots were used to illustrate the temperature dependence of ionic conductivity in all three fluoride garnets, which can be estimated using the equation $\sigma T = A \exp(-E_a/kT)$, where E_a is the activation energy, T is the absolute temperature, A is the pre-exponential factor, characteristic of the material, and k is the Boltzmann constant, respectively. Arrhenius plots are obtained for all three fluoride garnet compounds through heating and cooling cycles (Figure 4B). In the investigated temperature range between 100 and 300 °C, no considerable change in conductivity is seen during the heating and cooling cycles, suggesting that no distinct structural change in fluoride garnets occurs upon heating up to 300 °C. This confirms the good thermal stability of all three compounds. Moreover, the relation between $\log(\sigma T)$ vs $1000/T$ shows a slight bend at higher temperatures which may be caused by the order–disorder transition associated with the short-range ordering.[16] The calculated E_a for $Li_3Na_3Al_2F_{12}$, $Li_3Na_3Sc_2F_{12}$, and $Li_3Na_3In_2F_{12}$ are 0.95, 0.83, and 0.97 eV, respectively. These values are well-comparable to reported ideal oxide-based garnets (Table S2).[12,14]

A comprehensive analysis of the real part (Z') and imaginary part (Z'') of impedance further highlights the effect of cation deficiency on lithium-ion mobility. Archetypical plots of these analyses are presented in Figure 5. The fundamental relationship between complex impedance vs Z' and Z'' and their detailed evaluations are described systematically in previous reports.[24−27] Bode plots in Figure 5A–C show variation of Z' as a function of angular frequency (ω) at different temperatures for $Li_3Na_3M_2F_{12}$ (M = Al, Sc, In). Results show that the amplitude of Z' decreases with an increase in frequency and temperature. This is a typical occurrence in this class of materials and could indicate a lowering of the energy barrier and enhancement of conductivity across the grain boundaries at high frequencies and temperatures.[22,25] Several research groups have reported the same correlation (Z' vs ω at different temperatures).[22,27] They have suggested that a possible release of space charge results in lower barriers in these materials. The decrease in the value of Z' with temperature indicates the negative temperature coefficient of resistance behavior.[22] Panels D–F of Figure

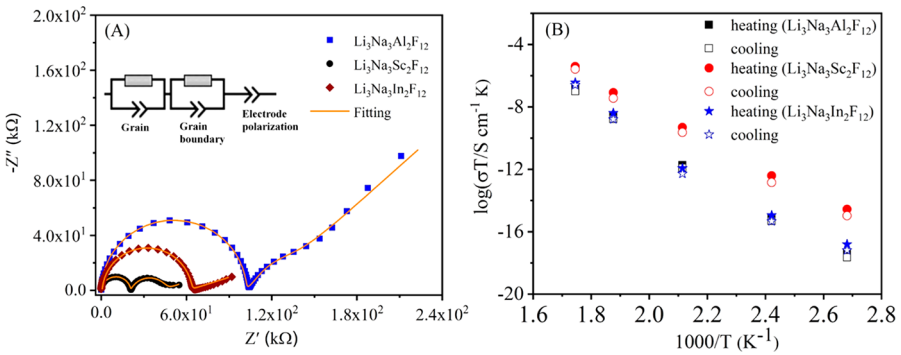

Figure 4. (A) Comparison of EIS Nyquist plots at 300 °C and (B) Arrhenius plots for $Li_3Na_3Al_2F_{12}$, $Li_3Na_3Sc_2F_{12}$, and $Li_3Na_3In_2F_{12}$ compounds.

Table 1. Variable Temperature Li^+ Ion Conductivity of Garnet-Type Lithium Metal Fluorides $Li_3Na_3Al_2F_{12}$, $Li_3Na_3Sc_2F_{12}$, and $Li_3Na_3In_2F_{12}$

	Conductivity at different temperatures (S/cm)							
Material	300 °C	260 °C	220 °C	200 °C	180 °C	140 °C	120 °C	100 °C
$Li_3Na_3Al_2F_{12}$	1.7×10^{-6}	3.8×10^{-7}	6.4×10^{-8}	3.5×10^{-8}	4.7×10^{-9}	5.5×10^{-10}	1.9×10^{-10}	1.2×10^{-10}
$Li_3Na_3Sc_2F_{12}$	8.2×10^{-6}	1.1×10^{-6}	1.6×10^{-7}	1.4×10^{-7}	2.3×10^{-8}	6.5×10^{-9}	3.2×10^{-9}	2.6×10^{-9}
$Li_3Na_3In_2F_{12}$	2.4×10^{-6}	2.9×10^{-7}	3.4×10^{-8}	9.5×10^{-9}	3.5×10^{-9}	5.2×10^{-10}	2.8×10^{-10}	1.8×10^{-10}

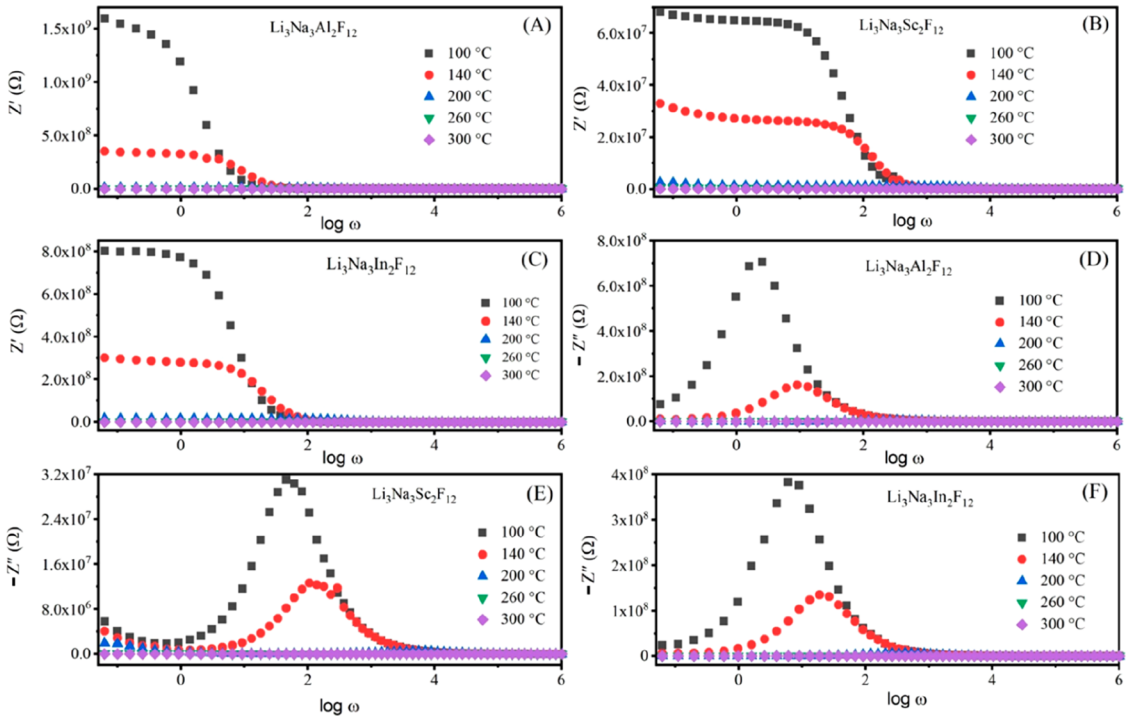

Figure 5. Variation of the imaginary component of impedance as a function of frequency (Z' vs log ω) for (A) $Li_3Na_3Al_2F_{12}$, (B) $Li_3Na_3Sc_2F_{12}$, and (C) $Li_3Na_3In_2F_{12}$. Variation of the imaginary component of impedance as a function of frequency (Z'' vs log ω) for (D) $Li_3Na_3Al_2F_{12}$, (E) $Li_3Na_3Sc_2F_{12}$, and (F) $Li_3Na_3In_2F_{12}$.

5 show variation in the Z'' as a function of angular frequency at different temperatures for $Li_3Na_3M_2F_{12}$ (M = Al, Sc, In). It can be seen from the curves that the Z'' value declines gradually with temperature in all three materials, suggesting the temperature dependence of relaxation phenomena within these materials. It also supports improved conductive properties of the materials. Further, the curves in plots of Z'' vs ω unveil a broad peak (known as the relaxation frequency) whose intensity and position change gradually with increasing temperature. The lower peak intensity indicates a high conductivity of the material and suggests the presence of nonmigratory (immobile) charged species.[22,25]

It has been reported that the ionic conductivity of garnet-type lithium oxides, $Li_{3+x}La_3M_2O_{12}$ (where M represents different metallic/metalloid cations and x is tuned according to the charge balance) significantly changed by increasing the lithium concentration through aliovalent substitutions at M and/or La sites.[14,28−30] Three prototypes of cubic garnet-type compounds $Li_3La_3Te_2O_{12}$ (LLT, $x = 0$), $Li_5La_3Nb_2O_{12}$ (LLN, $x = 2$), and $Li_7La_3Zr_2O_{12}$ (LLZ, $x = 4$) have widely been reported. In all compositions, different Li concentrations and their distributions have distinctly different ionic conductivities $\sigma_{LLT} \sim 0$ (as LLT behaves almost identically to other available Li_3 garnet compositions), $\sigma_{LLN} \sim 10^{-6}$ S/cm, and $\sigma_{LLZ} \sim 10^{-4}$ S/cm, at room temperature (RT).[28] The Li ions will preferentially occupy the tetrahedral position in $Li_{3+x}La_3M_2O_{12}$ garnet frameworks, and Li occupancy of the octahedral site occurs only after a concentration of >3 Li^+ per formula unit.[29,30] In order to increase the ionic conductivity of our fluoride garnets $Li_3Na_3M_2F_{12}$ (M = Al, Sc, In), we have tried to increase the Li concentration by aliovalent substitutions at the M and/or F sites. Particularly, the substitution of oxygen at F sites (i.e., $Li_{3+x}Na_3M_2F_{12-x}O_x$ ($0 \le x \le 2$)) not only increases Li concentration but also distributes Li ions at octahedral sites, thereby expecting ionic conductivity improvement in Li-rich fluoride garnets.

In summary, the crystal structures and ionic conductivity properties of a new class of garnet-type lithium metal fluorides $Li_3Na_3M_2F_{12}$ (M = Al, Sc, In) were described for SSBs. Our results indicate that fluoride garnets $Li_3Na_3M_2F_{12}$ are isostructural series to oxide garnets $Li_3Ln_3M_2O_{12}$ (Ln = lanthanides; M = Te, W). In this structure, Li^+ ions will preferentially occupy the tetrahedral site, and Li^+-ion occupation of the octahedral site starts only after a concentration of >3 Li^+ per formula unit is reached. The TGA results confirm that fluoride garnets are stable up to 650 °C. X-ray Rietveld refinement results confirm the formation of a cubic garnet structure with a space group $Ia\bar{3}d$ (No. 230). Scaling the AC conductivity spectrum ensures that temperature plays a significant role in Li^+-ion mobility and ionic

conductivity in fluoride garnets. The lithium ionic conductivities for $Li_3Na_3Al_2F_{12}$, $Li_3Na_3Sc_2F_{12}$, and $Li_3Na_3In_2F_{12}$ are 1.7×10^{-6}, 8.2×10^{-6}, and 2.4×10^{-6} S/cm at 300 °C, respectively. The E_a values for these compounds are found in the range of 0.83−0.97 eV. The variations of real and imaginary parts of impedance confirm the positive impact of higher lithium-ion concentration and distribution on the lithium-ion mobility in the $Li_3Na_3M_2F_{12}$ (M = Al, Sc, In). The ionic conductivity of these fluoride garnets can be further increased by increasing Li concentration in fluoride-based Li_3 garnets by filling the Li ions in octahedral sites, which can be possible by substituting oxygen at anion of fluorine and/or metal-ion substitution at cations sites.

AUTHOR INFORMATION

Corresponding Authors

Ediga Umeshbabu − *Helmholtz Institute Ulm (HIU) Electrochemical Energy Storage, 89081 Ulm, Germany; Institute of Nanotechnology, Karlsruhe Institute of Technology, D-76021 Karlsruhe, Germany;* orcid.org/0000-0003-4233-5565; Email: umeshbabu.ediga@kit.edu

Maximilian Fichtner − *Helmholtz Institute Ulm (HIU) Electrochemical Energy Storage, 89081 Ulm, Germany; Institute of Nanotechnology, Karlsruhe Institute of Technology, D-76021 Karlsruhe, Germany;* orcid.org/0000-0002-7127-1823; Email: m.fichtner@kit.edu

Anji Reddy Munnangi − *College of Engineering, Swansea University, Swansea SA1 8EN, United Kingdom;* orcid.org/0000-0001-9101-0252; Email: a.r.munnangi@swansea.ac.uk

Authors

Satyanarayana Maddukuri − *Department of Chemistry, Faculty of Exact Sciences, Bar-Ilan University, Ramat-Gan 5290002, Israel*

Doron Aurbach − *Department of Chemistry, Faculty of Exact Sciences, Bar-Ilan University, Ramat-Gan 5290002, Israel*

Notes

The authors declare no competing financial interest.

ACKNOWLEDGMENTS

This work contributes to the research performed at CELEST (Center for Electrochemical Energy Storage Ulm-Karlsruhe) and was funded by the German Research Foundation under Project ID 01DQ19012A (SELBA).

REFERENCES

(1) Janek, J.; Zeier, W. G. A Solid Future for Battery Development. *Nat. Energy* **2016**, *1*, 16141.

(2) Wu, J.; Yuan, L.; Zhang, W.; Li, Z.; Xie, X.; Huang, Y. Reducing the Thickness of Solid-State Electrolyte Membranes for High-energy Lithium Batteries. *Energy Environ. Sci.* **2021**, *14*, 12−36.

(3) Umeshbabu, E.; Zheng, B.; Yang, Y. Recent Progress in All-Solid-State Lithium-Sulfur Batteries Using High Li-Ion Conductive Solid Electrolytes. *Electrochem. Energy Rev.* **2019**, *2*, 199−230.

(4) Wu, B.; Wang, S.; Lochala, J.; Desrochers, D.; Liu, B.; Zhang, W.; Yang, J.; Xiao, J. The Role of the Solid Electrolyte Interphase Layer in Preventing Li Dendrite Growth in Solid-State Batteries. *Energy Environ. Sci.* **2018**, *11*, 1803−1810.

(5) Umeshbabu, E.; Zheng, B.; Zhu, J.; Wang, H.; Li, Y.; Yang, Y. Stable Cycling Lithium-Sulfur Solid Batteries with Enhanced Li/$Li_{10}GeP_2S_{12}$ Solid Electrolyte Interface Stability. *ACS Appl. Mater. Interfaces* **2019**, *11*, 18436−18447.

(6) Feinauer, M.; Euchner, H.; Fichtner, M.; Reddy, M. A. Unlocking the Potential of Fluoride-Based Solid Electrolytes for Solid-State Lithium Batteries. *ACS Appl. Energy Mater.* **2019**, *2*, 7196−7203.

(7) Hu, J.; Yao, Z.; Chen, K.; Li, C. High-conductivity Open Framework Fluorinated Electrolyte Bonded by Solidified Ionic Liquid Wires for Solid-State Li Metal Batteries. *Energy Storage Mater.* **2020**, *28*, 37−46.

(8) Li, X.; Liang, J.; Yang, X.; Adair, K.; Wang, C.; Zhao, F.; Sun, X. Progress and Perspectives of Halide-based Lithium Conductors for All-Solid-State Batteries. *Energy Environ. Sci.* **2020**, *13*, 1429−1461.

(9) Umeshbabu, E.; Maddukuri, S.; Hu, Y.; Fichtner, M.; Munnangi, A. Influence of Chloride Ion Substitution on Lithium-ion Conductivity and Electrochemical Stability in a Dual-Halogen Solid-State Electrolyte. *ACS Appl. Mater. Interfaces* **2022**, *14*, 25448−25456.

(10) Asano, T.; Sakai, A.; Ouchi, S.; Sakaida, M.; Miyazaki, A.; Hasegawa, S. Solid Halide Electrolytes with High Lithium-Ion Conductivity for Application in 4 V Class Bulk-Type All-Solid-State Batteries. *Adv. Mater.* **2018**, *30*, 1803075.

(11) Wells, A. F. *Structural Inorganic Chemistry*, 4th ed.; Clarendon Press: Oxford, U.K., 1975; p 500.

(12) O'Callaghan, M. P.; Lynham, D. R.; Cussen, E. J.; Chen, G. Z. Structure and Ionic-Transport Properties of Lithium-Containing Garnets $Li_3Ln_3Te_2O_{12}$ (Ln = Y, Pr, Nd, Sm-Lu). *Chem. Mater.* **2006**, *18*, 4681−4689.

(13) Murugan, R.; Weppner, W.; Schmid-Beurmann, P.; Thangadurai, V. Structure and Lithium Ion Conductivity of Garnet-Like $Li_5La_3Sb_2O_{12}$ and $Li_6SrLa_2Sb_2O_{12}$. *Mater. Res. Bull.* **2008**, *43*, 2579.

(14) Cussen, E. J.; Yip, T. W. S.; O'Neill, G.; O'Callaghan, M. P. A Comparison of the Transport Properties of Lithium-Stuffed Garnets and the Conventional Phases $Li_3Ln_3Te_2O_{12}$. *J. Solid State Chem.* **2011**, *184*, 470−475.

(15) Baral, A. K.; Narayanan, S.; Ramezanipour, F.; Thangadurai, V. Evaluation of Fundamental Transport Properties of Li-Excess Garnet Type $Li_{5+2x}La_3Ta_{2-x}Y_xO_{12}$ (x = 0.25, 0.5 and 0.75) Electrolytes Using AC Impedance and Dielectric Spectroscopy. *Phys. Chem. Chem. Phys.* **2014**, *16*, 11356−11365.

(16) Thangadurai, V.; Weppner, W. $Li_6ALa_2Nb_2O_{12}$ (A = Ca, Sr, Ba): A New Class of Fast Lithium Ion Conductors with Garnet-Like Structure. *J. Am. Ceram. Soc.* **2005**, *88*, 411−418.

(17) Zhu, M.; Pan, Y.; Xi, L.; Lian, H.; Lin, J. Design, Preparation, and Optimized Luminescence of A Dodec-Fluoride Phosphor $Li_3Na_3Al_2F_{12}$:Mn^{4+} for Warm WLED Applications. *J. Mater. Chem. C* **2017**, *5*, 10241−10250.

(18) Grzechnik, A.; Balic-Zunic, T.; Makovicky, E.; Gesland, J.-Y.; Friese, K. The Compressibility Mechanism of $Li_3Na_3In_2F_{12}$ Garnet. *J. Phys.: Condens. Matter.* **2006**, *18*, 2915−2924.

(19) Nicoll, J. S.; Gibbs, G. V.; Boisen, M. B.; Downs, R. T.; Bartelmehs, K. L. Bond Length and Radii Variations in Fluoride and Oxide Molecules and Crystals. *Phys. Chem. Miner.* **1994**, *20*, 617−624.

(20) Jonderian, A.; McCalla, E. The Role of Metal Substitutions in the Development of Li Batteries, Part II: Solid Electrolytes. *Mater. Adv.* **2021**, *2*, 2846−2875.
(21) Fanah, S. J.; Yu, M.; Huq, A.; Ramezanipour, F. Insight into Lithium-Ion Mobility in $Li_2La(TaTi)O_7$. *J. Mater. Chem. A* **2018**, *6*, 22152−22160.
(22) Fanah, S. J.; Yu, M.; Ramezanipour, F. Experimental and Theoretical Investigation of Lithium-ion Conductivity in $Li_2LaNbTiO_7$. *Dalton Trans.* **2019**, *48*, 17281−17290.
(23) Yip, T. W. S.; Cussen, E. J. Ion Exchange and Structural Aging in the Layered Perovskite Phases $H_{1-x}Li_xLaTiO_4$. *Inorg. Chem.* **2013**, *52*, 6985−6993.
(24) Fanah, S. J.; Ramezanipour, F. Lithium-Ion Mobility in Layered Oxide $Li_2(La_{0.75}Li_{0.25})(Ta_{1.5}Ti_{0.5})O_7$ Containing Lithium on both Intra and Inter-Stack Positions. *Eur. J. Inorg. Chem.* **2022**, *2022*, No. e202100950.
(25) Fanah, S. J.; Ramezanipour, F. Strategies for Enhancing Lithium-Ion Conductivity of Triple-Layered Ruddlesden-Popper Oxides: Case Study of $Li_{2-x}La_{2-y}Ti_{3-z}Nb_zO_{10}$. *Inorg. Chem.* **2020**, *59*, 9718−9727.
(26) Irvine, J. T. S; Sinclair, D. C.; West, A. R. Electroceramics: Characterization by Impedance Spectroscopy. *Adv. Mater.* **1990**, *2*, 132−138.
(27) Fanah, S. J.; Ramezanipour, F. Symmetry Effect on the Enhancement of Lithium-Ion Mobility in Layered Oxides $Li_2A_2B_2TiO_{10}$ (A = La, Sr, Ca; B = Ti, Ta). *J. Phys. Chem. C* **2021**, *125*, 3689−3697.
(28) Xu, M.; Park, M. S.; Lee, J. M.; Kim, T. Y.; Park, Y. S.; Ma, E. Mechanisms of Li^+ Transport in Garnet-Type Cubic $Li_{3+x}La_3M_2O_{12}$ (M = Te, Nb, Zr). *Phys. Rev. B: Condens. Matter Mater. Phys.* **2012**, *85*, No. 052301.
(29) Thangadurai, V.; Kaack, H.; Weppner, W. J. Novel Fast Lithium Ion Conduction in Garnet-type $Li_5La_3M_2O_{12}$ (M = Nb, Ta). *J. Am. Ceram. Soc.* **2003**, *86*, 437−440.
(30) Dong, B.; Yeandel, S. R.; Goddard, P.; Slater, P. R. Combined Experimental and Computational Study of Ce-Doped $La_3Zr_2Li_7O_{12}$ Garnet Solid-State Electrolyte. *Chem. Mater.* **2020**, *32*, 215−223.